RSC Advances

PAPER

View Article Online
View Journal | View Issue

Check for updates

Cite this: *RSC Adv.*, 2020, **10**, 36287

A series of guanidine salts of 3,6-bis-nitroguanyl-1,2,4,5-tetrazine: green nitrogen-rich gas-generating agent†

Zhang Cong,[a] Chen Xiang,[a] Hu Yongpeng,[a] Bai Yang,[a] Guo Zhaoqi,[a] Fan Daidi[bc] and Ma Haixia*[ab]

Nitrogen-rich energetic materials (EMs) have been widely studied because of their high thermal stability, insensitivity, excellent detonation performance and non-toxic characteristics. In particular, these compounds are well applied as gas-generating agents (GGAs). As a nitrogen-rich heterocyclic framework, 1,2,4,5-tetrazine derivatives have shown great potential in the design of GGAs. The guanidine salts of 3,6-bis-nitroguanyl-1,2,4,5-tetrazine (DNGTz), guanidine (G_2DNGTz) (**1**), aminoguanidine (AG_2DNGTz) (**2**), diaminoguanidine (DAG_2DNGTz) (**3**), and triaminoguanidine (TAG_2DNGTz) (**4**) have been synthesized and characterized by elemental analysis and FT-IR. The crystal structures of **1** and **2** were obtained by X-ray single crystal diffraction. Crystal analysis shows that **1** and **2** arrange through zigzag-chain-like assembly and face-to-face geometries, which is helpful in decreasing mechanical sensitivity. The thermal stability and thermal decomposition kinetics of these four salts were studied by Differential Scanning Calorimetry (DSC). Furthermore, the thermogravimetry-Fourier transform infrared-mass spectrometry (TG-FTIR-MS) analysis of thermal decomposition products reveals that the main decomposition gaseous products are H_2O, N_2O, CO_2, NO, N_2 and NH_3. Then, the cytotoxicity of the four salts was tested by MTT (3-(4,5-dimethyl-2-thiazolyl)-2,5-diphenyl-2-*H*-tetrazolium bromide) method, and it was found that salts **1–4** show slight cytotoxicity in mouse fibroblasts (L929), at a concentration of 0.125 mg ml^{-1}. The insensitivity, low toxicity, and production of clean gases without solid residue after burning of salt **1** indicate that it can be used as a potential green energetic material for GGAs.

Received 5th August 2020
Accepted 23rd September 2020

DOI: 10.1039/d0ra06766k

rsc.li/rsc-advances

Open Access Article. Published on 01 October 2020. Downloaded on 12/9/2025 10:25:56 PM.
This article is licensed under a Creative Commons Attribution-NonCommercial 3.0 Unported Licence.

Introduction

Recently, car accidents have been greatly increasing year-by-year. Therefore, it is strongly desired to develop inflatable air bags for protecting the human body from serious injury in the event of a collision. Different kinds of such air bags are in practical use.[1] Gas-generating sources are important in the device. Currently, most air bags are filled with solid gas-generating agents (GGAs) due to their high safety and reliability. The GGAs themselves and their decomposition products for expanding the air bag must be completely nontoxic, because they might possibly come into contact directly with the drivers and passengers if they should leak from the bag.[2] High nitrogen energetic molecules based on heterocyclic backbones have attracted much attention in recent years.[3] They have the advantages of higher positive heats of formation (HOF), insensitivity, good detonation performances and hypotoxicity.[4–7] As a high nitrogen heterocyclic framework, 1,2,4,5-tetrazine derivatives have shown great potential in the design of gas-generating agents due to the low combustion temperature, good mechanical properties, and production of clean gases without solid residue after decomposition, which is generally used as an inflation source in the airbag system.[8,9] A large amount of gases can be generated during the decomposition of medicament to inflate the generating device, so as to achieve the purpose of buffering.

As one of the representative tetrazine derivatives, 3,6-bis-nitroguanyl-1,2,4,5-tetrazine (DNGTz), can be used as a GGA. The HOF of DNGTZ is +389 kJ mol^{-1}, which is higher than of nitroguanidine (−98.7 kJ mol^{-1}), indicating that the introduction of tetrazine ring can greatly increase HOF.[10,11] In addition, it is insensitive to impact and friction stimuli (>14 J, 320 N).[12–14] These characteristics show that DNGTz is a prospective GGA with insensitivity.

At present, energetic ionic salts have attracted extensive interest, which outperform non-ionic molecules due to their lower vapor pressure and strong hydrogen bonding.[15–17] Among

[a]*School of Chemical Engineering, Northwest University Xi'an, Shaanxi, 710069, China. E-mail: mahx@nwu.edu.cn*

[b]*Shaanxi Key Laboratory of Degradable Biomedical Materials, School of Chemical Engineering, Northwest University, China*

[c]*Shaanxi R&D Center of Biomaterials and Fermentation Engineering, School of Chemical Engineering, Northwest University, China*

† Electronic supplementary information (ESI) available. CCDC 948107 and 953452. For ESI and crystallographic data in CIF or other electronic format see DOI: 10.1039/d0ra06766k

Open Access Article. Published on 01 October 2020. Downloaded on 12/9/2025 10:25:56 PM.
This article is licensed under a Creative Commons Attribution-NonCommercial 3.0 Unported Licence.

them, tetrazine-based ionic salts have high HOF and low carbon and hydrogen content to improve oxygen balance, showing promising potential to meet the needs of GGAs.[18–24]

In this paper, the guanidine salts of DNGTz, guanidine (G_2DNGTz) (**1**), aminoguanidine (AG_2DNGTz) (**2**), diaminoguanidine (DAG_2DNGTz) (**3**), triaminoguanidine (TAG_2DNGTz) (**4**) have been synthesized. The formation of guanidine salts could decrease acidic of DNGTZ and improve nitrogen content. The mainly decomposition products of salts **1–4** were investigated by thermogravimetry-Fourier transform infrared-mass spectrometry (TG-FTIR-MS) measurement to verify whether it contains toxic gases. Furthermore, to investigate the toxicity of four energetic salts, the MTT (3-(4,5-dimethyl-2-thiazolyl)-2,5-diphenyl-2-*H*-tetrazolium bromide) assay was used for the cytotoxicity experiment according to the ISO standards (ISO 10993.12-2005).

Experimental

Synthetic procedures

According to the ref. 6, the intermediate sodium-3,6-bis-nitroguanyl-1,2,4,5-tetrazine (Na_2DNGTz) was prepared. Other chemicals were purchased from Aladdin and used without further purification.

Na_2DNGTz (0.066 g, 0.2 mmol) was dissolved in 4 ml water and guanidine hydrochloride ($CH_5N_3 \cdot HCl$) (0.38 g, 4 mmol) (**1**) was dissolved in 2 ml water, then the latter solution was slowly added to the Na_2DNGTz aqueous solution and stirred for 2 h at 25 °C. The red precipitate was collected by filtration (Scheme 1). As for the preparation of salts **2–4**, the same procedure was adopted. Single crystals of **1** and **2** were obtained by slow evaporation in 2 days.

G_2DNGTz (**1**): IR (ATR), ν (cm^{-1}): 3390(w), 3149(m), 2970(m), 2364(s), 2326(m), 1726(w), 1485(s), 1215(m), 1062(w). Elemental analysis: calc. (%) for $C_6H_{16}N_{18}O_4$: C 17.82, N 62.38, H, 3.96; found: C 17.74, N 61.52, H 3.86. AG_2DNGTz (**2**): IR (ATR), ν (cm^{-1}): 3390, 3143, 2964, 2364, 2362, 1726, 1487, 1211 1062. Elemental analysis: calc. (%) for $C_6H_{18}N_{20}O_4$: C, 16.59; N, 64.51; H, 4.15. Found: C, 16.89; N, 63.65; H, 3.89. DAG_2DNGTz (**3**): IR (ATR), ν (cm^{-1}): 3417, 3147, 2964, 2360, 2331, 1726, 1485, 1220, 1065. Elemental analysis: calc. (%) for $C_6H_{20}N_{22}O_4$: C 15.52, N 66.38, H 4.31; found: C 15.55, N 65.51, H 3.88. TAG_2DNGTz (**4**): IR (ATR), ν (cm^{-1}): 3408, 3145, 2968, 2356, 2324, 1726, 1481, 1215,1063. Elemental analysis: calc. (%) for $C_6H_{22}N_{24}O_4$: C 14.57, N 68.02, H 4.05; found: C 14.38, N 67.01, H 4.81.

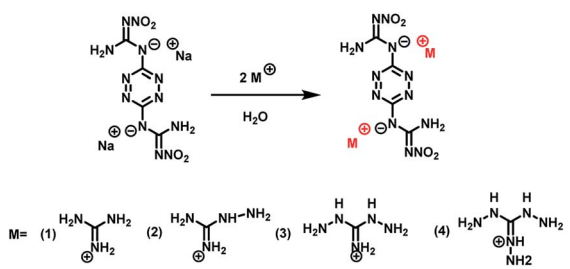

Scheme 1 Synthetic route of salts **1–4**.

Materials and physical measurements

Elemental Analyses (EA) were performed on a Vario EL Analyzer. Infrared (IR) spectra were measured with ATR using IRAffinity-1S apparatuses. The crystal morphology was observed by Scanning Electron Microscope. DSC measurements were performed on Q2000 apparatus under nitrogen atmosphere with the flowing rate of 50 ml min^{-1}. TG-MS-FTIR was performed using Mettler TGA/DSC3+ HT/1600, Thermo Fisher NICOLET iS10 and Pfeiffer Vacuum GSD 320 T3. Two gas pipelines (N_2 and Ar) were assembled to steer gaseous products from TG to FTIR and MS simultaneously. Under the constant N_2 flowing rate (100 ml min^{-1}), the temperature was 40 to 300 °C at a heating rate of 10 °C min^{-1}. The impact sensitivity test was performed on a ZBL-B impact sensitivity instrument.

X-ray crystallography

A red plate (0.31 × 0.25 × 0.14 mm^3) (**1**) and a red block (0.37 × 0.30 × 0.14 mm^3) (**2**) were used for the X-ray crystallographic analysis. X-ray diffraction data were collected on a Bruker Smart Apex CCD X-ray diffractometer. The structures were solved by the direct methods using SHELXS-97 and refined by the full matrix least-squares method on F^2 with anisotropic thermal parameters for all non-H atoms (SHELXTL-97),[25] and H atoms were added according to the theoretical models. Crystal data are listed in Table 1. Selected bond lengths angles are listed in Tables S1 and S2,† respectively. CCDC 948107 and CCDC 953452.

Cytotoxicity test (MTT assay)

In vitro cytotoxicity test, Mouse Fibroblast (L929) cells were propagated and maintained in cell culture dishes and seeded to wells. L929 cells were seeded on plates at a density of 10^4 cells per well (100 μL). The multi-well plates were incubated at 37 ± 1 °C, air (5% CO_2) for 24 h. The cultures were replaced with 100 μL media at four different concentrations: 100%, 50%, 25%, 12.5%. Similarly, cultures were replaced with 100 μL of positive control (DMSO 10%, 5%, 2,5%, 1.25%) and 100 μL of the reagent control (RPMI-1640) and 100 μL of negative control. The wells were incubated at 37 ± 1 °C in 5% CO_2 for 24 ± 0.5 hours. Following incubation, the cultures were examined microscopically (Olympus IX-51) to evaluate cellular characteristics. The cultures were then prepared for an MTT assay by aspirating the media and then adding 20 μL MTT in culture media to the volume of cells and keeping in a dark environment for 24 h at 37 °C. Subsequently, MTT was aspirated and 150 μL DMSO was added to each well. Then, the absorbance at 490 nm was measured using a Thermo Scientific Microplate Reader (Bio Tek). MTT assays were repeated in three separate experiments.

Results and discussion

Crystal structure

The morphology of salts **1–4** were studied by SEM measurements. As shown in Fig. S1,† it could be clearly seen that **1** forms plate-like crystal with a smooth surface. **3** and **4** show rod-like crystalline morphology. While, **2** crystalizes in small particles.

 This journal is © The Royal Society of Chemistry 2020

Open Access Article. Published on 01 October 2020. Downloaded on 12/9/2025 10:25:56 PM.
This article is licensed under a Creative Commons Attribution-NonCommercial 3.0 Unported Licence.

Table 1 X-ray diffraction data collection and refinement parameters for salts **1** and **2**

	1	**2**
Formula	$C_6H_{16}N_{18}O_4$	$C_6H_{16}N_{20}O_4$
Formula weight	404.37	434.40
Crystal system	Monoclinic	Triclinic
Temperature (K)	296.15	296.15
Space group	$P2_1/c$	$P\bar{1}$
a/(Å)	8.4812(18)	7.4720(16)
b (Å)	24.898(5)	7.8861(16)
c/(Å)	7.7969(16)	8.2265(18)
α/(°)	90.00	80.222(4)
β/(°)	95.961(4)	64.653(3)
γ/(°)	90.00	84.717(4)
ρ	1.640	1.671
Z	4	1
F (000)	840	226
θ range/(°)	1.64, 25.10	2.77, 25.09
R indices ($I > 2\sigma(I)$)	$R_1 = 0.0552$, $wR_2 = 0.0855$	$R_1 = 0.0713$, $wR_2 = 0.1601$
R indices (all data)	$R_1 = 0.1191$, $wR_2 = 0.1047$	$R_1 = 0.1100$, $wR_2 = 0.1844$
GOOF	1.030	1.036
CCDC	948107	953452

Crystal structures of G_2DNGTz (**1**) and AG_2DNGTz (**2**) are shown in Fig. 1. Both **1** and **2** have the 2 : 1 of cation and anion in the crystal structure. In the DNGTZ anions ($DNGTZ^{2-}$), the lengths of N–C and N–N are within 1.316–1.400 Å and 1.306–1.332 Å, which is longer than normal N=C, N=N bond (1.22 Å, 1.20 Å) and shorter than normal N–C,N=N bond (1.47 Å, 1.41 Å) (Tables S1 and S2†).[26,27] These results prove that $DNGTZ^{2-}$ exists as a large π-conjugated system.

G_2DNGTz (**1**) crystallized in the monoclinic space group $P2_1/c$ with a density of 1.640 g cm^{-3} (Fig. 1(1a)). The amine and nitro groups of $DNGTZ^{2-}$ form hydrogen bonds with the N atoms of guanidine anions (G^+). Besides, these extensive inter- and intramolecular hydrogen bonds between $DNGTZ^{2-}$ and G^+ not only support a planar structure by forming a five- and six-member hydrogen-bonds rings, but also improve the thermal stability and decrease mechanical sensitivity (Fig. 2(1b) Table S3†). The dihedral angles: N1–N2–C1–N3 (0.9(5)) and N8–N7–C2–N5 (0.2(5)) are almost zero, which shows that $DNGTZ^{2-}$ has a planar structure. In addition, the hydrogen atoms from amino groups participate in large numbers of hydrogen bonds with the nearby nitrogen and oxygen atoms, thereby forming a zigzag-chain-like structure along the a-axis (Fig. 3(1c)).

AG_2DNGTz (**2**) crystallized in the triclinic space group $P\bar{1}$ with a density of 1.671 g cm^{-3} at 296 K (Fig. 1(2a)). All atoms of the $DNGTZ^{2-}$ are almost coplanar, for the biggest deviation of the torsion angles is 4.3° (O2–N1–N2–C1). The molecular moieties are involved in extensive hydrogen bonding network through the hydrogen atoms of the amine groups and nitrogen and oxygen atoms of AG^+ and $DNGTZ^{2-}$ (Fig. 2(2b)). The crystal structure of **2** features face-to-face geometries with the interlayer distance of 3.489 Å and the π-stacked sheets were arranged in a layer-like structure (Fig. 3(2c)). Among them, the π-stacked layers were deemed to decrease the mechanical sensitivity by converting mechanical energy into intermolecular interaction energy.[28]

To further understand the interactions between the molecules contained in **1** and **2**, the Hirschfeld surface (d_{norm} (Fig. 4(d)) shape index (Fig. 4(e)), curvedness (Fig. S2†))and 2D fingerprint plots were analyzed.[29] As shown in Fig. 4(d), the surfaces of **1** and **2** have a plate shapes because of the conjugated molecular structures and most of the red dots indicating close molecular contact between molecules are located on the side of the plate. It indicates that the intermolecular interactions in the crystal structure occur through the oxygen and nitrogen atoms surrounding the molecules. The curvedness surfaces show broad, relatively flat regions characteristic of planar stacking. Furthermore, complementary red and blue triangles (outlined by two white rectangles) can be identified on the shape index plots, which can be considered as π stacking interactions in a plane. The 2D fingerprint of the populations of these weak interactions is shown in Fig. 4(f) and (g). It observed that two sharp spikes existed in the bottom left of the spectra, indicating the interactions of O···H and N···H. Among them, the interaction of N···H (and H···N) (37.6% and 36.3%) was much higher than that of O···H (23.8% and 24.1%), showing the main interactions of the energetic molecules were N···H interactions.

Thermal behaviors and non-isothermal kinetics

DSC analysis was used to investigate the thermal decomposition behaviors of salts **1–4**. As can be seen the DSC curves in Fig. 5, all of the materials exhibit high decomposition temperatures over 180 °C, satisfying the thermal stability requirements for GGAs. And only one exothermic process with the peak of 189.2 to 239.3 °C can be observed for salts **1–4**. Salt **1** has the best thermal stability and the decomposition peak temperature is 239.3 °C. The results show that as the hydrogen on guanidine

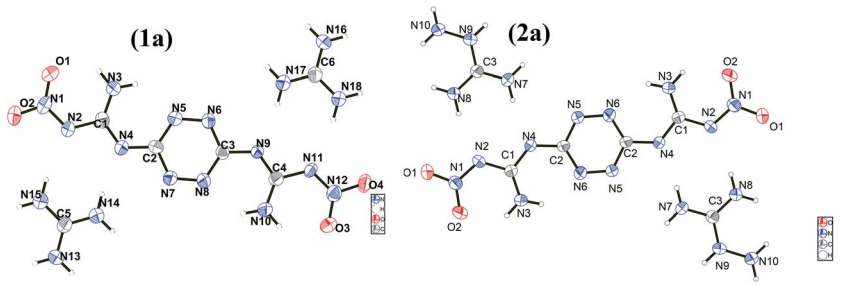

Fig. 1 Crystal structure of G_2DNGTz (**1**) and AG_2DNGTz (**2**).

Open Access Article. Published on 01 October 2020. Downloaded on 12/9/2025 10:25:56 PM.
This article is licensed under a Creative Commons Attribution-NonCommercial 3.0 Unported Licence.

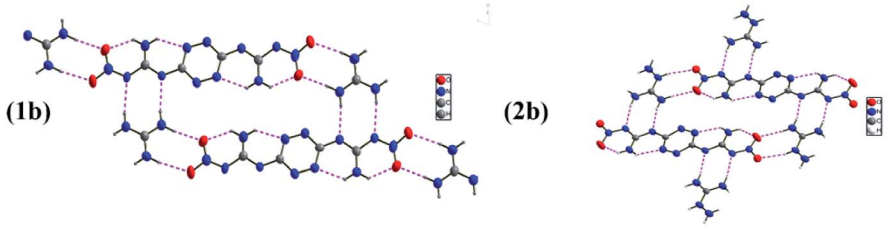

Fig. 2 Two-dimensional structure of G_2DNGTz (**1**) and AG_2DNGTz (**2**).

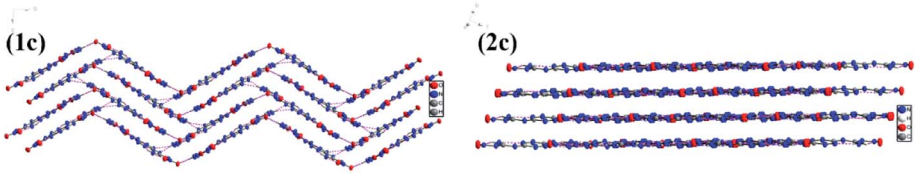

Fig. 3 Packing diagram of G_2DNGTz (**1**) and AG_2DNGTz (**2**).

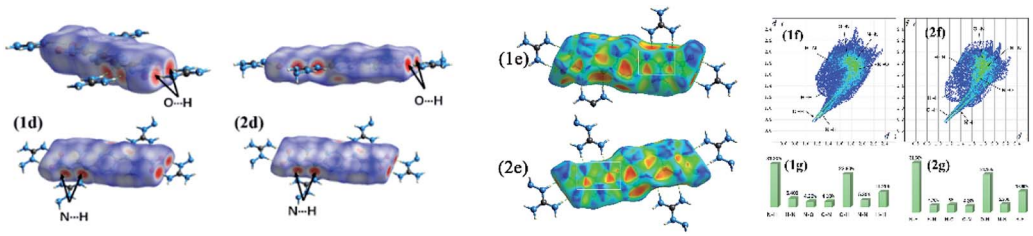

Fig. 4 Hirshfeld surfaces mapped with d_{norm} (d) and shape index (e) of G_2DNGTz (**1**) and AG_2DNGTz (**2**). The 2D fingerprint plots (f) for G_2DNGTz (**1**) and AG_2DNGTz (**2**). Percentage contributions of the individual atomic contacts to the Hirshfeld surface (g) for G_2DNGTz (**1**) and AG_2DNGTz (**2**), respectively.

group is gradually replaced by amino group in salts **1–4**, the thermal decomposition temperature decreases and the exothermic decomposition process accelerates.

In order to estimate non-isothermal kinetics of salts **1–4** during the exothermic decomposition process, the kinetic parameters have been calculated through Kissinger method and Ozawa method (eqn (1) and (2)) at different T_p (maximum decomposition peak temperature).[30,31] The kinetic parameters are listed in Table 2.

$$\ln \frac{\beta}{T_p^2} = \ln \frac{AR}{E} - \frac{E}{RT_p} \quad (1)$$

$$\lg \beta + \frac{0.4567E}{RT} = C \quad (2)$$

where β (°C min^{-1}) is the heating rate, R (8.314 J K^{-1} mol^{-1}) is the gas constant and C is a constant, E is the apparent activation energy (kJ mol^{-1}) and A is pre-exponential constant.

Thermal safety analysis

To further evaluate their thermal safety, the critical temperature of thermal explosion (T_b), entropy of activation ($\Delta S^{\neq}$), enthalpy of activation ($\Delta H^{\neq}$) and free energy of activation ($\Delta G^{\neq}$) of salts **1–4** were obtained from eqn (3)–(7).[32] The thermal parameters are listed in Table 3. According to Table 3, T_b of salts **1–4** is within the range of 177.15–229.47 °C, and the results reveal that the order of thermal stabilities of these energetic salts is: **1** > **2** > **3** = **4**. The positive values of $\Delta G^{\neq}$ (193.56–378.53 kJ mol^{-1}) and $\Delta H^{\neq}$ (128.61–142.93 kJ mol^{-1}) of salts **1–4**, show that the exothermic decomposition reaction of salts **1–4** must proceed under heating condition. At the same time, the greater the values of $\Delta G^{\neq}$ and $\Delta H^{\neq}$, the greater the external energy required for material decomposition, and the more stable it is under the same external thermal stimulation condition. The $\Delta G^{\neq}$ and $\Delta H^{\neq}$ of salts **2–4** are less than **1**, indicating the highest thermal safety of **1**.

$$T_{pi} = T_{p0} + a\beta_i + b\beta_i^2 \quad i = 1\text{–}4 \quad (3)$$

$$T_b = \frac{E_O - \sqrt{E_O^2 - 4E_O RT_{p0}}}{2R} \quad (4)$$

where a and b are coefficients, β is the linear heating rate.

$$A = \frac{k_B T}{h} \exp\left(\frac{\Delta S^{\neq}}{R}\right) \quad (5)$$

$$\Delta H^{\neq} = E_a - RT \quad (6)$$

$$\Delta G^{\neq} = \Delta H^{\neq} - T\Delta S^{\neq} \quad (7)$$

 This journal is © The Royal Society of Chemistry 2020

Open Access Article. Published on 01 October 2020. Downloaded on 12/9/2025 10:25:56 PM.
This article is licensed under a Creative Commons Attribution-NonCommercial 3.0 Unported Licence.

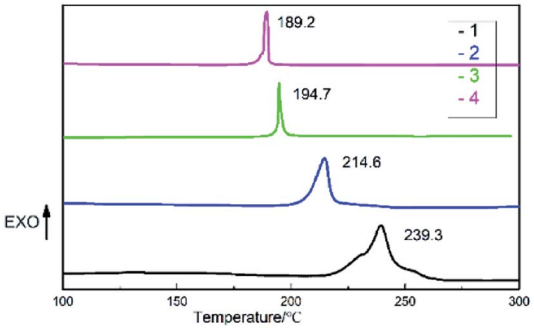

Fig. 5 DSC curves of salts **1–4** at a heating rate of 10 °C min^{-1}.

where $T = T_{p0}$, $E_a = E_K$ and $A = A_K$. k_B is the Boltzmann constant (1.381×10^{-23} J K^{-1}) and h is the Planck constant (6.626×10^{-34} J s).

Decomposition gas products analysis by TG-MS-FTIR

TG-MS-FTIR were used to analyze the thermal decomposition process and identify gaseous products during the thermal decomposition of reference compounds. Fig. 6–9 shows the thermal decomposition process of salts **1–4** in the temperature range of 30–300 °C.

In the TG thermograms (Fig. 6), mass loss process of salt **1** mainly occurred from 228.41 to 245.33 °C, reaching maximum mass loss rate at 240.55 °C, with a weight loss percentage of 35.27%. Similarly, the exothermic peak temperature of salts **2–4** was found at 213.48, 194.18 and 188.36 °C with a weight loss percentage of 22.39%, 29.17% and 36.74%, showing the rapid weight loss process (204.62 to 219.58 °C, 190.19 to 196.89 °C and 186.28 to 191.39 °C). These results show that when the hydrogen on the guanidyl group is gradually replaced by the amino group, the weight loss process is gradually shortened and the weight loss rate is accelerated. For all compounds, the temperature range of mass loss processes was found to be in agreement with that of the exothermic processes.

Table 3 Calculated values of kinetic parameters of decomposition reaction for salts **1–4**

	T_{p0}/°C	T_b/°C	$\Delta S^{\neq}$/J mol^{-1} K^{-1}	$\Delta H^{\neq}$/kJ mol^{-1}	$\Delta G^{\neq}$/kJ mol^{-1}
1	228.57	229.47	469.59	378.53	142.93
2	202.77	203.99	210.78	236.39	136.08
3	176.46	177.57	152.27	197.39	128.93
4	176.02	177.15	144.60	193.56	128.61

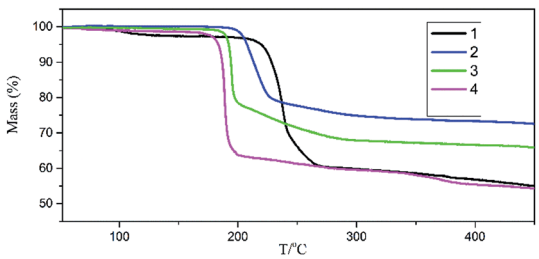

Fig. 6 TG curves of salts **1–4** at a heating rate of 10 °C min^{-1}.

The evolved gaseous products during the decomposition processes of salts **1–4** were detected by quadrupole mass spectrometry(MS) and FT-IR. From Fig. 7–9, we can deduce that the main decomposition products of salts **1–4** are NH_3 (ν = 3334–3330, 967–963 and 932–928 cm^{-1}, m/z = 16, 17), H_2O (m/z = 18), N_2 (m/z = 14,28), NO (ν = 1831–1825 cm^{-1}, m/z = 30), N_2O (ν = 2206–2204 and 2237–2239 cm^{-1}, m/z = 44) and CO_2 (ν = 2349–2347 cm^{-1}, m/z = 44). When the temperature reached to T_p, infrared signals were nearly vanished, there by proving that salts **1–4** were completely decomposed. Besides, with the increasing of heating temperature, HCN (ν = 713 cm^{-1}, ν = 681 cm^{-1}, m/z = 27) can be detected during the decomposition of salts **3** and **4**. The thermal decomposition rates of salts **1–4** show the order of **1** < **2** < **3** < **4**.

Table 2 Kinetic parameters from the exothermic decomposition reaction for **1–4** at various heating rates

	β/°C min^{-1}	T_p/°C	E_K kJ^{-1} mol^{-1}	log(A_K/s^{-1})	r_K	E_O/kJ mol^{-1}	r_O
1	5	234.40	382.71	37.55	0.9936	372.01	0.9939
	10	238.54					
	15	241.00					
	20	241.77					
2	5	210.07	240.35	24.01	0.9909	236.28	0.9915
	10	214.74					
	15	219.36					
	20	220.49					
3	5	184.54	201.13	20.93	0.9970	198.59	0.9972
	10	191.18					
	15	194.10					
	20	196.34					
4	5	183.7	197.30	20.52	0.9968	194.93	0.9970
	10	190.43					
	15	193.09					
	20	195.84					

Open Access Article. Published on 01 October 2020. Downloaded on 12/9/2025 10:25:56 PM.
This article is licensed under a Creative Commons Attribution-NonCommercial 3.0 Unported Licence.

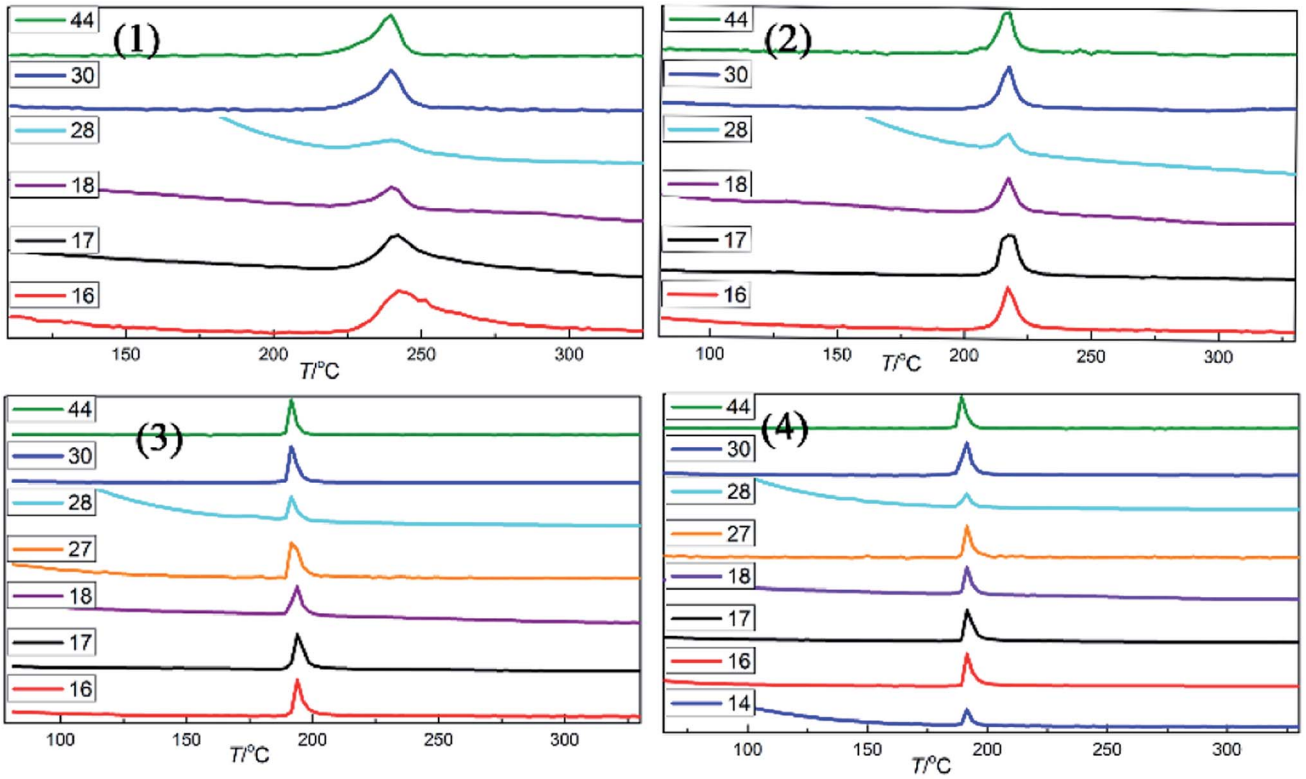

Fig. 7 MS spectra of detected gaseous products for thermolysis of salts **1–4**.

Cytotoxicity test

In addition to pursued nontoxic decomposition products, low cytotoxicity has also become a consideration for designing GAAs. Lately, M. Gozin reported cytotoxicity in Normal Human Dermal Fibroblasts (NHDF) cells results for some energetic compounds, using alamar-Blue assay.[28] According to the ISO standards (ISO 10993.12-2005), the MTT assay was used for the

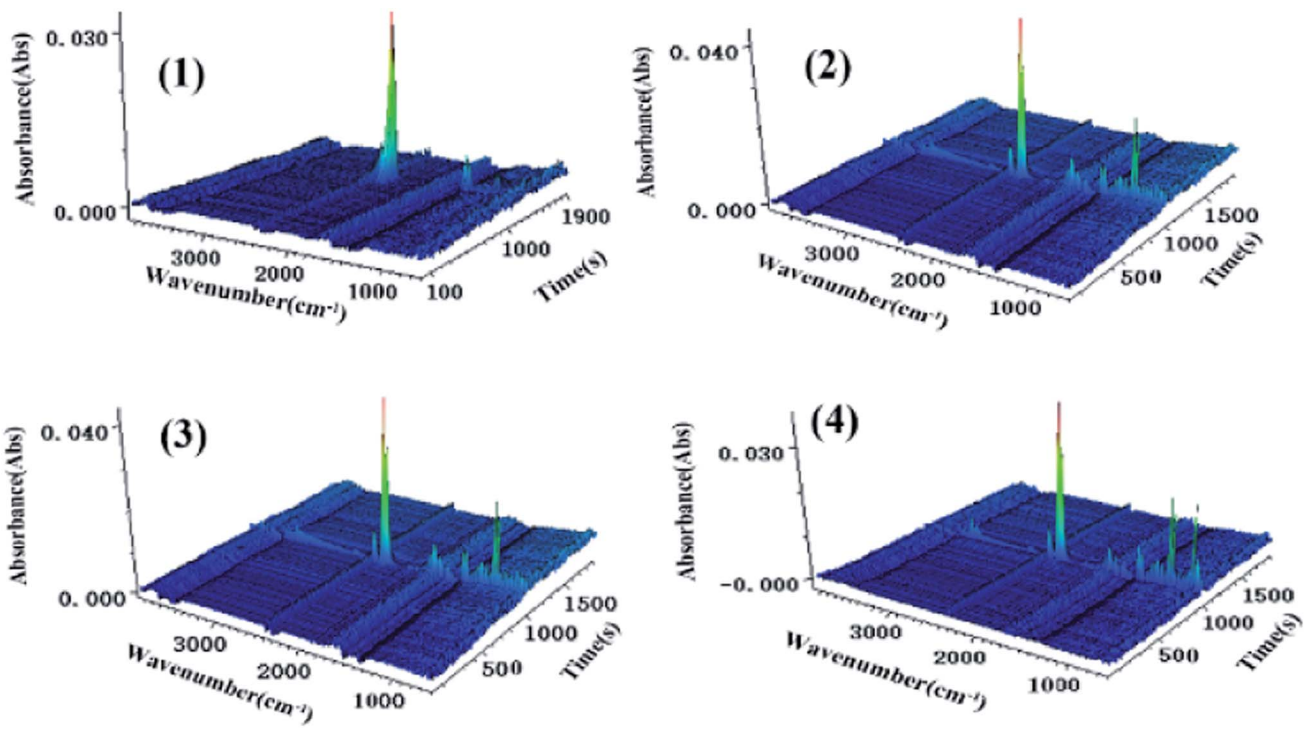

Fig. 8 3D FTIR spectra of salts **1–4** thermal decomposition with the heating rate of 10 °C min^{-1}.

 This journal is © The Royal Society of Chemistry 2020

Open Access Article. Published on 01 October 2020. Downloaded on 12/9/2025 10:25:56 PM.
This article is licensed under a Creative Commons Attribution-NonCommercial 3.0 Unported Licence.

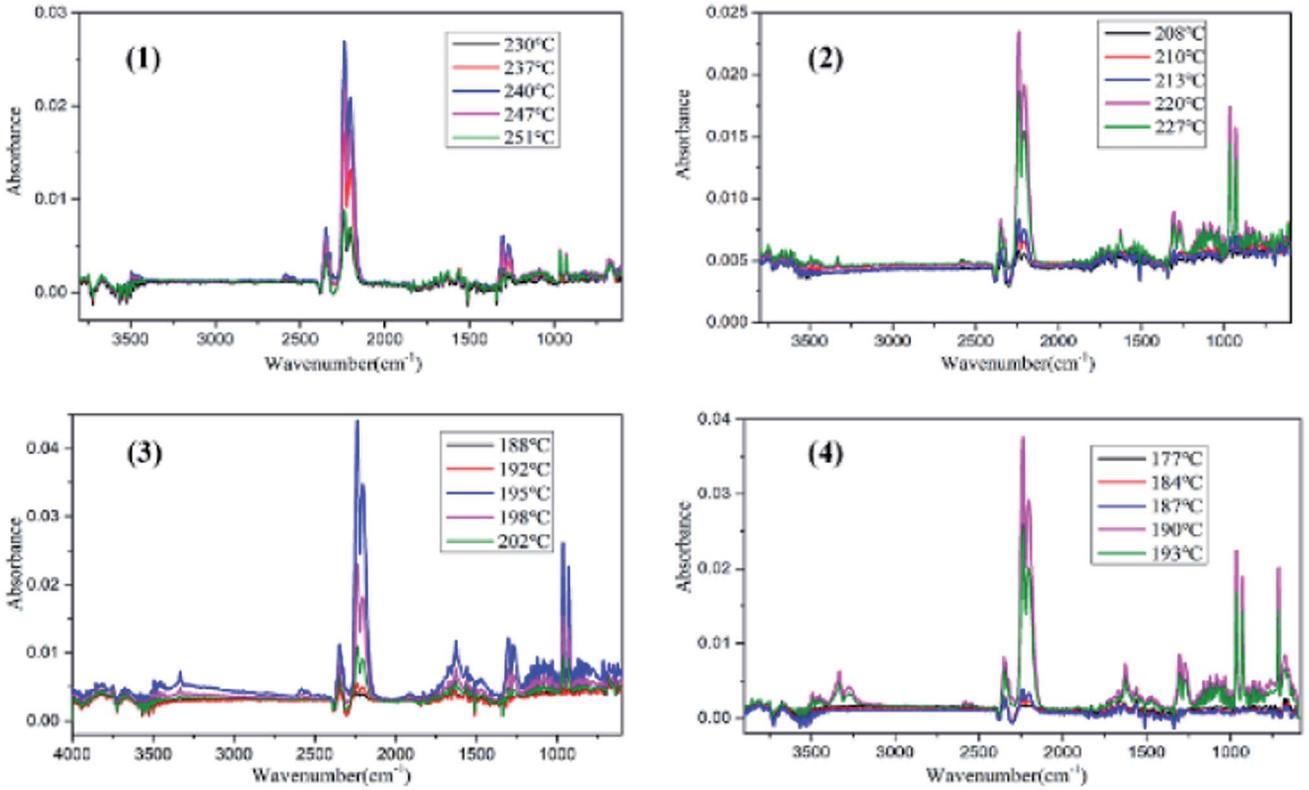

Fig. 9 FT-IR spectra of the gaseous products for thermolysis of salts.

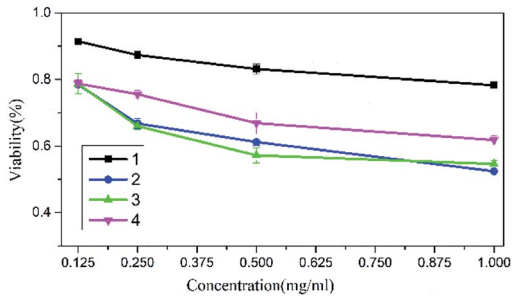

Fig. 10 Results of cytotoxicity tests for salts **1–4**.

cytotoxicity experiments of **1–4** (Fig. S3†). We found that all salts show slight cytotoxicity in mouse fibroblasts (L929) at 0.125 mg ml^{-1}. And that, with the increase of salt concentration, the activity of cells decreases. Salt **1** was found to be the safest compound in the cytotoxicity test with the L929 cells viability of above 75% at a salt concentration of 1 mg ml^{-1}. While the **2–4** were found to have similar toxicity, with L929 cells viability of above 52–60% at 1 mg ml^{-1} (Fig. 10).

Impact sensitivity

Sensitivity is an important property for GGAs during storage and transportation. The impact sensitivity (IS) for salts **1–4** was determined by fall hammer method using 2 kg drop weight with maximum height of 120 cm. No explosion was detected after 10 time strikes which means the compound has the IS value larger than 24 J. By pairing with nitrogen-rich anions, the energetic salts are well stabilized with additional ionic and hydrogen bonding, thus the four salts could be classified as insensitive compounds.

Conclusions

In summary, four energetic ionic salts based on DNGTz were synthesized and characterized by EA and FT-IR. The crystal structures of G_2DNGTz (**1**) and AG_2DNGTz (**2**) were obtained by X-ray single crystal diffraction and the crystal densities are 1.640 (**1**) and 1.671 (**2**) g cm^{-3}, respectively. When the hydrogen on the guanidyl group is gradually replaced by the amino group, the T_p, E_a and T_b gradually decreases. Besides, TG-FTIR-MS analyses show that the main decomposition gas products of salts **1–4** are H_2O, N_2, CO_2, and NH_3. Furthermore, the cytotoxicity of the four salts were tested by MTT method, and it is found that all the compounds show slight cytotoxicity in mouse fibroblasts (L929), at concentration of 0.125 mg ml^{-1}. Additionally, the impact sensitivity of salts **1–4** are >24 J. The insensitivity, low toxicity, production of clean gases and without solid residue after burning of salt **1** indicate that it can be used as a potential green energetic material for gas generating agents.

Conflicts of interest

There are no conflicts to declare.

Open Access Article. Published on 01 October 2020. Downloaded on 12/9/2025 10:25:56 PM.
This article is licensed under a Creative Commons Attribution-NonCommercial 3.0 Unported Licence.

Acknowledgements

This work is supported by the National Natural Science Foundation of China (No. 21673179) and the Natural Science Foundation of Shaanxi Province (No. 2020JZ-43).

Notes and references

1 (*a*) S. R. Ganta, C. G. Miller and G. K. Williams, *US Pat.* US2009/008002A1,2009; (*b*) S. Tomiyama and J. Wu. *US Pat.* US7811397B2,2010.
2 (*a*) A. N. Ali, S. F. Son, M. A. Hiskey and D. L. Naud, *J. Propul. Power*, 2012, **20**, 120; (*b*) A. Hammerl, M. A. Hiskey, G. Holl, T. M. Klapotke, K. Polborn, J. R. Stierstorfer and J. J. Weigand, *Chem. Mater.*, 2005, **17**, 3784.
3 (*a*) A. Aizikovich, A. Shlomovich, A. Cohen and M. Gozin, *Dalton Trans*, 2015, **44**, 13939; (*b*) T. W. Myers, K. E. Brown, D. E. Chavez, R. J. Scharff and J. M. Veauthier, *Inorg Chem*, 2017, **56**, 2297.
4 T. W. Myers, J. A. Bjorgaard, K. E. Brown, D. E. Chavez, S. K. Hanson, R. J. Scharff, S. Tretiak and J. M. Veauthier, *J. Am. Chem. Soc.*, 2016, **138**, 468.
5 (*a*) H. X. Ma, B. Yan, Z. N. Li, Y. L. Guan, J. R. Song, K. Z. Xu and R. Z. Hu, *J. Hazard. Mater.*, 2009, **169**, 1068; (*b*) R. Hu, Z. Yang and Y. Liang, *Thermochim. Acta*, 1988, **134**, 429.
6 D. E. Chavez, M. A. Hiskey and R. D. Gilardi, *Org. Lett.*, 2004, **6**, 2889.
7 (*a*) H. X. Gao, C. F. Ye, C. M. Piekarski and J. M. Shreeve, *J. Phys. Chem. C*, 2007, **111**, 10718; (*b*) D. E. Chavez, M. A. Hiskey and D. L. Naud, *Propellants, Explos., Pyrotech.*, 2004, **29**, 209; (*c*) H. Wei, H. Gao and J. M. Shreeve, *Chem.–Eur. J.*, 2014, **20**, 16943.
8 A. Saikia, R. Sivabalan, B. G. Polke, G. M. Gore, A. Singh, A. S. Rao and A. K. Sikder, *J. Hazard. Mater.*, 2009, **170**, 306.
9 H. R. Blomquist. *US Pat.* US6113713, 2000.
10 D. E. Chavez, B. C. Tappan, M. A. Hiskey, S. F. Son, H. Harry, D. Montoya and S. Hagelberg, *Propellants, Explos., Pyrotech.*, 2005, **30**, 412.
11 Q. Zhang, C. He, P. Yin and J. M. Shreeve, *Chem.–Asian J.*, 2014, **9**, 212.
12 J. Li, H. Ma, B. Yan, A. Yang, T. Mai and L. Bai, *Chin. J. Explos. Propellants*, 2010, **33**, 1.
13 D. E. Chavez, M. A. Hiskey, M. H. Huynh, D. L. Naud, S. F. Son and B. C. Tappan, *J. Pyrotech.*, 2006, **23**, 70.
14 Y. Hu, X. Zhao, N. Zhao, B. Yan, H. Gao, F. Zhao, R. Hu, J. Song and H. Ma, *Chin. J. Energ. Mater.*, 2014, **22**, 767.
15 W. Li, J. J. Tian, X. J. Qi, K. C. Wang, Y. H. Jin, B. S. Wang and Q. H. Zhang, *ChemistrySelect*, 2018, **3**, 849.
16 Z. Q. Guo, Y. Wang, X. M. Liu, C. Zhang, Y. Z. Zhang and H. X. Ma, *CrystEngComm*, 2019, **21**, 462.
17 J. C. Zhang, J. H. Zhang, D. A. Parrish and J. M. Shreeve, *J. Mater. Chem. A*, 2018, **6**, 22705.
18 Y. L. Liu, G. Zhao, Y. X. Tang, J. C. Zhang, L. Hu, G. H. Imler, D. A. Parrish and J. M. Shreeve, *J. Mater. Chem. A*, 2019, **7**, 7875.
19 S. Lei, B. Jin, R. F. Peng, Q. C. Zhang and S. J. Chu, *J. Coord. Chem.*, 2017, **70**, 2384.
20 T. H. Zhang, J. Du, Z. M. Li, X. Y. Lin, L. Wang, L. Yang and T. L. Zhang, *CrystEngComm*, 2019, **21**, 765–772.
21 W. Bo, Z. Wang, H. Yang, Q. Lin and G. Cheng, *New J. Chem.*, 2015, **39**, 893.
22 J. Zhou, S. J. Wu, W. H. Zhang, Q. Liu, B. Yang, Y. H. Ren, H. X. Ma, F. Q. Zhao and R. Z. Hu, *Chem. Res. Chin. Univ.*, 2019, **35**, 403.
23 Z. M. Li, S. H. Xie, J. G. Zhang, J. L. Feng, K. Wang and T. L. Zhang, *J. Chem. Eng. Data*, 2012, **57**, 729.
24 X. H. Jin, B. C. Hu, Z. L. Liu and C. X. Lu, *Chin. J. Explos. Propellants*, 2014, **37**, 18.
25 (*a*) G. M. Sheldrick, *SHELXS-97, Program for the Solution of Crystal Structures*, University of Göttingen, Germany, 1997; (*b*) G. M. Sheldrick, *SHELXL-97, Program for the Refinement of Crystal Structures*, University of Göttingen, Germany, 1997.
26 Q. Q. Qiu, K. Z. Xu, S. H. Yang, Z. Gao, H. Zhang, J. R. Song and F. Q. Zhao, *J. Solid State Chem.*, 2013, **205**, 205.
27 Z. B. Zhang and J. G. Zhang, *J. Mol. Struct.*, 2018, **1158**, 88.
28 A. Shlomovich, T. Pechersky, A. Cohen, Q. L. Yan, M. Kosa, N. Petrutik, N. Tal, A. Aizikovich and M. Gozin, *Dalton Trans.*, 2017, **46**, 5994.
29 (*a*) M. A. Spackman and J. J. Mckinnon, *CrystEngComm*, 2002, **4**, 378; (*b*) J. J. McKinnon, D. Jayatilaka and M. A. Spackman, *Chem. Commun.*, 2007, **37**, 3814; (*c*) M. A. Spackman and P. G. Byrom, *Chem. Phys. Lett.*, 1997, **267**, 215.
30 E. H. Kissinger, *Anal. Chem.*, 1957, **29**, 1702–1706.
31 T. Ozawa, *Bull. Chem. Soc. Jpn.*, 1965, **38**, 1881–1886.
32 (*a*) R. Hu, Z. Yang and Y. Liang, *Thermochim. Acta*, 1988, **123**, 131; (*b*) T. Zhang, R. Hu, X. Yi and F. Li, *Thermochim. Acta*, 1994, **244**, 171.

 This journal is © The Royal Society of Chemistry 2020